

First-principles study on energetics of *c*-BN(001) reconstructed surfaces

Jun Yamauchi* and Masaru Tsukada

Department of Physics, Faculty of Science, University of Tokyo, Hongo, Tokyo 113, Japan

Satoshi Watanabe[†]

*Aono Atomcraft Project, Exploratory Research for Advanced Technology, Research Development Corporation of Japan (JRDC),
Kaga 1-7-13, Itabashi-ku, Tokyo 173, Japan*

Osamu Sugino

NEC, 34 Miyukigaoka, Tsukuba 305, Japan

(Received 18 December 1995)

Total energies of cubic boron nitride (*c*-BN) (001) surfaces are systematically studied for various reconstructed configurations by the local density-functional approach with ultrasoft pseudopotentials. Stable phases as a function of nitrogen chemical potential are predicted theoretically. We examine the validity of the electron counting (EC) rule, which plays an important role for the study of the GaAs surfaces, and obtain supplemental factors to determine stable surface structures. The results of the total-energy minimization calculation demonstrate that the EC rule holds very well within the models that contain at most one layer with defects and no interlayer N-N and B-B bonds, and that next to the EC rule, the electrostatic energy has the most important role in determining stable structures. Furthermore, in the nitrogen-rich region, we found that the EC rule does not hold, because the energy difference between the N-B and N-N bonds is larger than the energy gain from using the EC model. We suggest that the important factors for determining stable structures of the *c*-BN(001) surface are N-B bond saturation, the EC rule, and electrostatic energy, whose effect decreases in this order. The difference between *c*-BN and GaAs surfaces is also discussed. [S0163-1829(96)01723-7]

I. INTRODUCTION

Boron nitride (BN) has a phase diagram that is similar to that of carbon, that is, hexagonal BN (*h*-BN), cubic BN (*c*-BN), and wurtzite BN (*w*-BN) which correspond to the graphite, diamond, and hexagonal diamond structures of carbon, respectively. Among these polymorphs, *c*-BN, which is also called *borazon*, is an exotic material with a zinc-blende structure, that is, the stable phase at high pressure and high temperature, and is metastable under ordinary conditions. Unlike diamond, *c*-BN does not exist in nature. Historically *c*-BN was synthesized under high pressure and high temperature conditions by Wentorf in 1956.¹ The properties of *c*-BN are very attractive from both scientific and technological viewpoints. *c*-BN is the second hardest material following diamond and is used as a protective coating material.² For the purpose of fabricating semiconducting devices working under high temperature, *c*-BN shows fascinating features, such as high thermal conductivity, semiconducting properties with a wide energy gap, low dielectric constant, high melting point, etc. Although it is difficult to dope stable *n*-type impurities in diamond, we can make both *p* and *n*-type *c*-BN. Furthermore, since the lattice constant of *c*-BN is larger than that of diamond by only 1.3%, *c*-BN is a promising substrate material for the growth of heteroepitaxial chemical vapor deposition (CVD) films of diamond. Thanks to these properties, *c*-BN can be applied to exotic semiconducting devices.

In recent years, *c*-BN has attracted much interest since its synthesis has been successfully realized by CVD (Ref. 3) and physical vapor deposition (PVD) (Refs. 4–11) techniques.

For a review, refer to Ref. 2. Study of heteroepitaxial growth using *c*-BN as a substrate or a growth material has been a current trend. Typical examples are diamond on *c*-BN(111) by dc plasma CVD (Ref. 12) and *c*-BN(100) on Si(100).¹³ The latter is characterized by 3:2 commensurate lattice matching. To understand the growth of *c*-BN, it is very important to determine stable structures and properties of the *c*-BN surfaces. Unlike Si and GaAs, the growth of *c*-BN is performed under conditions where its phase is metastable. Therefore the growth of the metastable phase can be attributed to the surface condition.

As for the theoretical aspects, bulk *c*-BN has been studied energetically with the first-principles calculations using the local density approximation (LDA) and by other methods for fifteen years. These include studies of the electronic structure and crystal structures with LCAO (linear combination of atomic orbitals) calculations,¹⁴ LCAO Hartree-Fock,^{15,16} first-principles pseudopotential (PP) calculations,^{17–21} full-potential linear augmented plane-wave method,²² and *ab initio* self-consistent orthogonalized LCAO method.²³ The band gap of the (110) diamond-*c*-BN superlattice has been studied with the linear augmented plane-wave method.²⁴ Recently some bulk properties were calculated with ultrasoft pseudopotentials.²⁵ On the other hand, since it is very difficult to prepare high-quality clean surfaces of *c*-BN, there are few experiments to characterize the surface, for example, by low-energy electron diffraction (LEED) and scanning tunneling microscopy (STM). Thus, as a first step toward recognition of the growth mechanism, a theoretical study of the reconstructed *c*-BN surface has a fundamental significance. However, although many interesting experiments on epitax-

ial growth have been reported in recent years, there are few theoretical studies of the surfaces. Furthermore, no first-principles studies have been reported as far as we know. This is attributed to the difficulty of first-principles calculations. In the study of surfaces, which have a low symmetry compared to the bulk crystal, it is necessary to minimize the total energy with respect to the ionic configuration and to obtain reconstructed surface structures.

In this work, c -BN(001) reconstructed surfaces are studied by first-principles calculations with ultrasoft pseudopotentials as proposed by Vanderbilt,²⁶ which overcome many of the difficulties of the conventional norm-conserving PP. As for the preliminary works, see Refs. 27 and 28. To allow efficient optimization, conjugate gradient methods are used for the total-energy minimization with respect to the wave functions and the positions of the ions. Using these methods we study the reconstructed surface structures with different stoichiometries to clarify the properties of c -BN(001) surfaces. As mentioned above, there are few experiments that give information about the surface reconstructions. Therefore, we have to calculate the surfaces of c -BN with various kinds of symmetries: (1×1) , (2×1) , $c(2 \times 2)$, (2×2) , and (2×4) for both boron- and nitrogen-rich surfaces.

To begin with, we optimized the structures of the (2×1) and $c(2 \times 2)$ reconstructions for both B and N (001) surfaces without vacancies. For these symmetries it is expected that the dimer structure should be favorable as is the case of (001) surfaces of Si, Ge, and GaAs. On the other hand, a semiempirical study²⁹ predicts that (2×1) nitrogen-terminated surfaces favor the bridge structure, which is suggested as the model for the carbon-terminated SiC $c(2 \times 2)$ surface by experiments³⁰ and semiempirical calculations.³¹ Therefore, optimization was performed for these two models. However, the result turns out to be contrary to that obtained by the semiempirical calculation. From our calculation the bridge structure has much higher energy than the dimer structure. This difference is attributed to the different calculational methods. From the results for the surface without vacancies, we construct models taking the dimer structure as a stable constituent.

Based on the calculated results, the stability of the models is discussed for various stoichiometries. Furthermore, the validity of the electron counting (EC) model for the c -BN surface is discussed, since the EC rule has been successful in the explanation of the reconstruction of GaAs surfaces.^{32,33} If its validity is confirmed, the EC model will be an effective guiding principle for experiments and theoretical studies of c -BN(001) surfaces.

The organization of this work is as follows. In Sec. II, the calculational method and a test of the ultrasoft pseudopotentials are briefly described. Section III is devoted to the description of the models used in this study. Further, the calculated results and the characteristic features of each reconstructed structure are shown in Sec. IV. In Sec. V, the stability of the structures for the different stoichiometries is investigated and the validity of the EC rule in c -BN(001) is also discussed. In the last section, the results are summarized.

II. METHODS OF CALCULATION

In this section, we describe the calculational method used to minimize the total energy with respect to the positions of

ions and the tests of the PP's for B and N. We adopt the local density-functional formalism^{34,35} with the PP approximation. The total energy and the Hellmann-Feynman forces are obtained from first-principles calculations with the ultrasoft PP (UPP) suggested by Vanderbilt.^{26,36} Since the UPP's show good transferability without norm conserving and produce smooth pseudo-wave-functions, it is feasible to perform first-principles calculations of materials containing first row elements such as boron and nitrogen. For the pseudo-wave-functions, we adopt Troullier and Martins type³⁹ functions *without* the norm-conserving condition. For the exchange-correlation term, we adopted Ceperley-Alder type³⁷ parameterized by Perdew and Zunger,³⁸ unless noted otherwise. The total energy is minimized with respect to the positions of the ions by the conjugate gradient method (CG).⁴⁰ The CG method is also applied to the Kohn-Sham equation for the electronic degrees of freedom.⁴¹ We apply the CG algorithm of Bylander, Kleinman, and Lee⁴² with preconditioning⁴³ to the generalized eigenvalue problem. To save computational cost, we did the optimization in two steps.^{44,45} In the first step, we performed geometry optimization with a soft PP of nitrogen with $R_c(\text{core radius})=1.6$ a.u. and $E_c(\text{cutoff energy})=20.25$ Ry. In the next step, we further optimize the structure by a hard and more accurate PP with $R_c=1.2$ a.u. and $E_c=36$ Ry starting from the geometry determined by the first step. The PP of boron with $R_c=1.2$ a.u. is adopted for both steps. Furthermore, in the second step, we exclude some models that have much higher energies than the others in the first step calculation.

The calculational conditions are as follows: the numbers of irreducible k points sampled in the Brillouin zone are 32(16), 16(8), 16(8), 32(20), 8(4), 4(2), and 4(2) for (1×1) , (2×1) , (1×2) , $c(2 \times 2)$, (2×2) , (2×4) , and (4×2) unit cells, respectively, where the numbers in the parentheses are those for the models with mirror symmetries. The criterion of convergence in the geometry optimization is that the forces on all the atoms that are allowed to move are less than 1×10^{-3} Hartree/a.u.

Since various configurations of atoms are allowed in the surfaces, the PP's should be tested in various environments. Therefore, we calculated physical quantities for several materials including boron and nitrogen. Unless otherwise noted, the calculation is executed with the single-reference UPP's with a core radius $R_c=1.2$ a.u. for boron and 1.2 and 1.6 a.u. for nitrogen, respectively. The cutoff energy is taken as 36.00 Ry for the system using nitrogen PP ($R_c=1.2$) and as 20.25 Ry for the other systems. These are the conditions used in the present study and also used in the later study.

For nitrogen, tests were done on a diatomic molecule and α -N₂. For the N₂ molecule the interatomic distance and the vibrational frequency are calculated in a $10 \times 10 \times 10$ a.u.³ supercell. The α -N₂, which is the ground state of solid nitrogen, has a strange structure where the centers of N₂ constitute an fcc lattice with a unit cell containing 4 N₂, and each N₂ molecule is aligned to a different (111) direction.⁴⁶ The results are summarized in Table I. The agreement between the experiments and the present calculations is excellent except for the lattice constant of α -N₂. Although the calculated values are improved for the nitrogen PP with $R_c=1.2$, the evident difference ($\sim 8\%$) between the experiments and the present work still remains. This discrepancy

TABLE I. Calculated structures of nitrogen. The values in the parentheses denote core radii (R_c) in atomic units. Cutoff energies are 36.00 Ry for nitrogen PP ($R_c=1.2$) and 20.25 Ry for ($R_c=1.6$), respectively.

N_2 molecule	Bond length (a.u.)	$\hbar\omega$ (cm^{-1})
Expt. ^a	2.07	2359
LCAO(LSDA) ^b	2.08	2387
Present(1.6)	2.06	2389
Present(1.2)	2.06	2441

α - N_2	Lattice constant (a.u.)	N_2 bond length (a.u.)
Expt. ^c	10.68	2.02
Present (1.6)	9.55	2.09
Present (1.2)	9.77	2.04

^aReference 47.

^bReference 48.

^cReference 49.

could be attributed to the LDA, because α - N_2 is a typical molecular crystal. Probably the generalized gradient approximation⁵⁰ and other extensions of LDA would recover the short lattice constant.

Comparing to the structures of nitrogen, those of solid boron are much more exotic, where the B_{12} icosahedron is the unit of the structure. The calculation is done for α -boron, which has a rhombohedral structure made of B_{12} icosahedra. In the present calculation, the lattice constant is calculated as $a_h=4.83$ Å, where the rhombohedral unit cell is approximately regarded as a hexagonal unit cell and the ratio a/c is fixed throughout the calculation. The values determined by experiments^{51,52} are $a_h=4.927$ and $c_h=12.564$ Å. The relative difference between the experimental and the theoretical values is within 2%, which is an acceptable value.

For h -BN, which has a structure similar to graphite, the a and c axes are both optimized. The results are listed in Table II. The lattice constant for the a axis (intraplane) is

TABLE II. The calculated results for h -BN. As for the calculational condition, see the caption of Table I.

Lattice constant (Å)	a axis	c axis
Expt. ^a	2.5040	6.661
Present(1.6)	2.49	6.33
Present(1.2)	2.48	6.45

^aReference 51.

reproduced well. However, with the more plausible PP ($R_c=1.2$), that for the c axis (interplane) is still slightly shorter (3%) than the experimental value. This may be attributed to the failure of the LDA when applied to the interlayer region with a dilute electron density, as is the case of α - N_2 .

Since c -BN is the main target in this study, the bulk modulus and its derivatives are obtained by Murnaghan fitting⁵³ as is the lattice constant. The results are tabulated in Table III. As mentioned before, in this work the correlation term is taken as Ceperley-Alder type. There is a little discrepancy between the present result and that by Knittle, Wentzcovitch, Jeanloz, and Cohen.²⁰ This difference is attributed to the different exchange-correlation functional forms, not to the difference of PP's, because the result with the Wigner interpolation formula⁵⁵ as the correlation term gives an excellent correspondence to their result as well as the experimental one. Therefore the difference is a measure of ambiguity in the LDA. Moreover, this table contains the results for PP's with single and double reference energies with $R_c=1.6$ and it is found that little difference can be seen in terms of the lattice constant and the bulk modulus and its derivatives for c -BN.

III. MODELS

Since a c -BN(001) surface consists of layers containing only B or N atoms, depending on the stacking of the B and N layers, the electrostatic field due to charge transfer is induced

TABLE III. The calculated results for c -BN. Unless otherwise noted, Murnaghan's equations are used to fit data. The values in the parentheses denote core radius (R_c) in atomic units. Cutoff energies are 36.00 Ry for nitrogen PP ($R_c=1.2$) and 20.25 Ry for ($R_c=1.6$), respectively. W and CA denote Wigner and Ceperley-Alder type exchange-correlation term. See text.

	Lattice constant (Å)	B_0 (GPa)	B'_0	Notes
Expt. ^a	3.615(± 0.002)	369(± 14)	4.0(± 0.2)	Birch fit ^b
LCAO ^{a,c}	3.618(± 0.008)	370(± 10)	3.1(± 0.1)	W
Present(1.2)	3.578	394	3.2	CA
Present(1.6)	3.580	399	3.1	CA
Present(1.6) ^d	3.580	399	3.1	CA
Present(1.2)	3.615	374	3.1	W
Present(1.6)	3.624	378	3.0	W

^aReference 20.

^bReference 54.

^cLDA.

^dWith double reference energies.

in both the slab and the vacuum region. To avoid this artificial charge transfer, we adopt a model with *virtual* hydrogen terminators with $1.25e$ valence charge, which has been successfully applied to GaAs.⁵⁶ These terminators terminate the dangling bonds on the other surface and suppress the unphysical charge transfer between the back and front surfaces. From calculating the Hellmann-Feynman forces, we have found that a virtual hydrogen atom with $1.25e$ valence charge is a more efficient terminator than the other candidates such as virtual H with $0.75e$, virtual Li with 3.25 and $2.75e$, fractionally charged B and N, etc. These models fail to reproduce the forces, which act on the B and N atoms with large unit cells. However, the states derived from the virtual hydrogen atoms appear in the gap region. This is not the case for GaAs, because the band gap of GaAs is much smaller than that of c -BN. In spite of this difficulty, we adopt this model for the following reason. The virtual H states are unoccupied and only weakly hybridize with the surface states on the other side. This is because the surfaces are spatially well separated. The virtual hydrogen model with two BN layers reproduces the forces of slab models with four BN layers without the terminators, within $\sim 1.0 \times 10^{-3}$ Hartree/a.u. The direction of the virtual hydrogen is assigned as it is for the bulk silicon bond. The bond length between a virtual hydrogen and a boron atom is determined as 1.862 a.u. by total-energy minimization. We also tested the effect of the thickness of the vacuum region on the Hellmann-Feynman forces and found that the gap width corresponding to five layers is enough to obtain the above accuracy. Therefore, we adopt repeated slab models terminated by virtual hydrogen atoms. This model contains six layers of B and N for nitrogen-rich surfaces and five for boron-rich surfaces in a supercell corresponding to 13 layers, where the thickness of one layer is equivalent to 1.6915 a.u. The bottom two layers containing the virtual hydrogen terminators are fixed throughout the total-energy minimization processes.

In the present work, we used models with various kinds of symmetries. Furthermore, since c -BN(001) consists of layers containing only B or N atoms, B- and N-rich surfaces have to be investigated with different coverages. Surfaces with $\theta=0.25, 0.50, 0.75$, and 1.00 are systematically investigated, where θ is the coverage, and some models with higher coverages are also studied. It is convenient to briefly summarize the models for the c -BN(001) surface and the terms referring to configurations used in this work. The model for the N-rich surface of each coverage is introduced in the following. The correspondent structure for the B-rich surface is obtained by a $\pi/2$ rotation.

For convenience, we define *flat* models as those that contain at most one layer with defects. In the present study we investigate the *flat* models systematically. Unless otherwise mentioned, we deal with flat models. In the following description, *ideal* means the atomic configuration in which the atoms are located at the position of an ideal bulk, *relaxed* means the configuration where the atoms are relaxed from the ideal configuration without a reconstruction to another symmetry, and a *hollow* site is the center of four atoms in the second layer.

For full coverage ($\theta=1.00$), Fig. 1 illustrates schematically the top views of the models: (a) (1×1) ideal, (b) (2×1) dimer, (c) (1×2) bridge, (d) $c(2 \times 2)$ dimer, and (e)

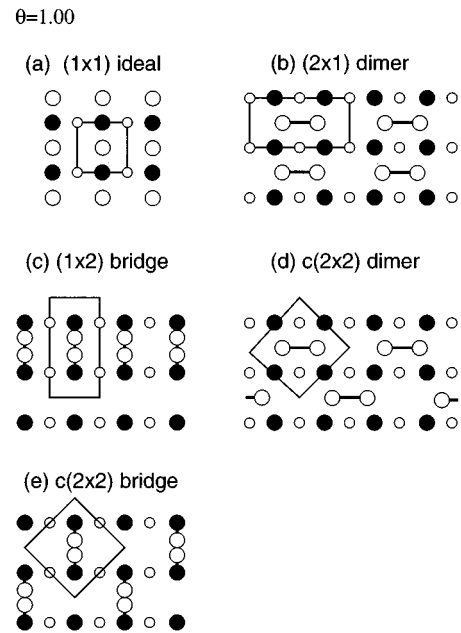


FIG. 1. Schematic illustration of the top views of the models for full coverage ($\theta=1.00$): (a) (1×1) ideal; (b) (2×1) dimer; (c) (1×2) bridge; (d) $c(2 \times 2)$ dimer; (e) (2×2) bridge, respectively. The open, closed, and small open circles indicate the atoms in the first, second, and third layers, respectively. Dimer and bridge bonds are indicated with thick solid lines. The rectangles refer to a unit cell for each configuration.

$c(2 \times 2)$ bridge, respectively. The open, closed, and small open circles indicate the atoms in the first, second, and third layers, respectively. Dimer and bridge bonds are indicated with thick solid lines. The rectangles refer to a unit cell for each configuration. These notations are also used in Figs. 2 and 3. With these unit cells, two fundamental structures are adopted as the models, dimer and bridge structures. The dimer structures, whose top views are shown in Figs. 1(b) and 1(d), and side view in Fig. 4(a), are widely observed in the (001) surfaces of semiconductors with a tetrahedral structure such as Si, Ge, C, GaAs, etc. The surfaces of Si(001) exhibit an asymmetric dimer structure and those of GaAs(001) a symmetric one. Therefore, symmetric and asymmetric dimer models are examined for the (2×1) and the $c(2 \times 2)$ unit cells.

In the bridge structures, a diatomic molecule is inserted into the dimer bond and makes a bridge between the two dimer atoms in the second layer as shown in Figs. 1(c) and 1(e) (top views), and in Fig. 4(b) (side view). These structures were suggested for c -BN(001)- (1×2) N-rich surfaces from semiempirical calculations,²⁹ and were originally suggested for SiC(001)- $c(2 \times 2)$ C-rich surfaces from experiments³⁰ and a semiempirical calculation.³¹ Thus we optimized the $c(2 \times 2)$ model as well as the (1×2) model. In accord with Ref. 29, we call the bridge models with d_2 larger than d_3 type I, and those with the opposite relation, ($d_2 < d_3$), we call type II. The values d_2 and d_3 are defined in Fig. 4(b).

Besides the above-mentioned symmetries, the (2×2) bridge and dimer models are investigated, since the asymmetric $p(2 \times 2)$ structures are more favorable than the (2×1) , (1×2) , and $c(2 \times 2)$ structures in terms of the bond

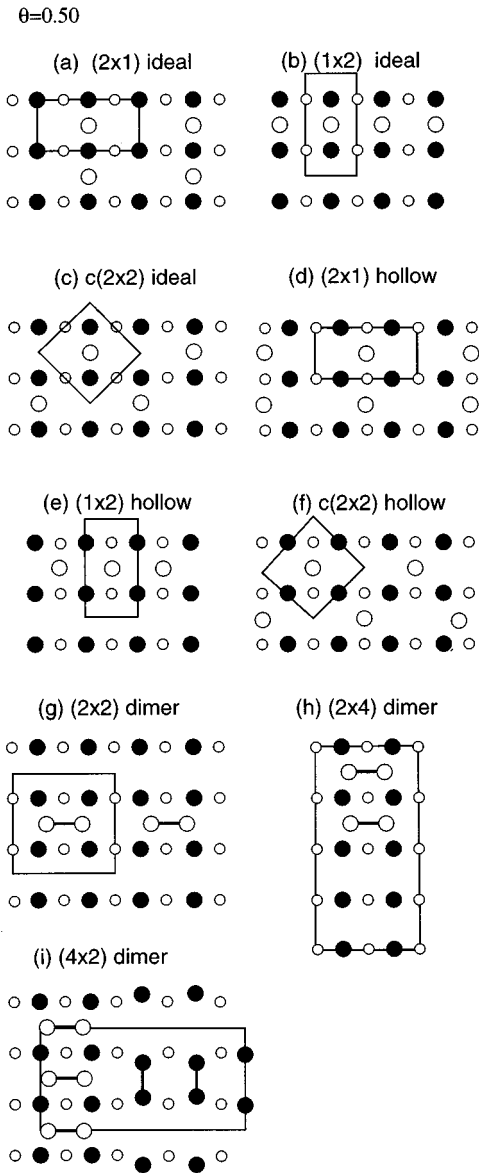


FIG. 2. Schematic illustration of the top views of the models for half coverage ($\theta=0.5$): (a) (2×1) ideal; (b) (1×2) ideal; (c) $c(2 \times 2)$ ideal; (d) (2×1) hollow; (e) (1×2) hollow; (f) $c(2 \times 2)$ hollow; (g) (2×2) dimer; (h) (2×4) dimer, (i) (4×2) dimer, respectively. See text.

distortion. However, as will be discussed in Sec. IV, the asymmetric structures will turn out not being favored in the present calculations. Furthermore, the bridge structures have much higher energy by about 1 eV than the dimer structures. Therefore we adopted the symmetric dimer structure as the basic unit of larger models with different coverage ($\theta=0.25, 0.50, 0.75$).

For half coverage ($\theta=0.50$), various configurations with small unit cells are realized for this coverage such as (2×1) , (1×2) , and $c(2 \times 2)$. The calculated models are the ideal, relaxed, and hollow structures with (2×1) , (1×2) , and $c(2 \times 2)$, respectively, as well as (2×2) , (2×4) , and (4×2) dimer structures. These models are summarized in Fig. 2, where the relaxed structures are not shown because these have the same schematic configurations as the ideal ones.

For $\theta=0.25$ and 0.75 coverages, the smallest unit cells

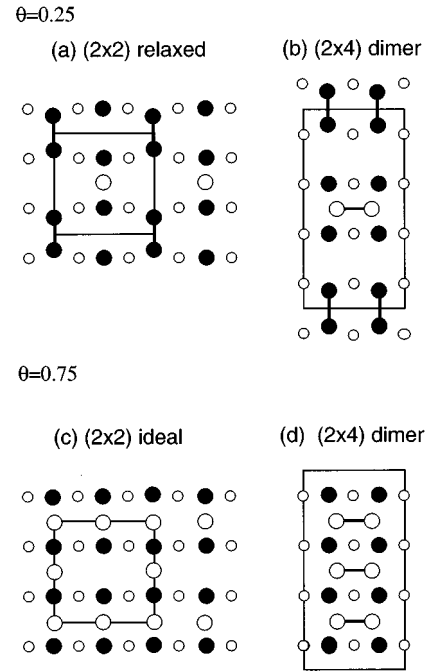


FIG. 3. Schematic illustration of the top views of the models for $\theta=0.25$: (a) (2×2) relaxed; (b) (2×4) dimer, and for $\theta=0.75$: (c) (2×2) ideal; (d) (2×4) dimer. See text.

with these coverages are (2×2) , (4×1) , and (1×4) . Since the size of computation is larger than that of the case with $\theta=0.50$ and 1.00 , we must select the favorable models. The models are illustrated in Fig. 3. These models are based on the dimer structures. For $\theta=0.25$, the (2×2) relaxed structure [Fig. 3(a)] is a combination of the dimer and the relaxed structure. Further, the (2×4) dimer structure [Fig. 3(b)] also consists of dimers with relaxation, since the relaxed structures are found to be as stable as dimer-based ones; see Sec. IV. For $\theta=0.75$, the (2×4) missing dimer structure [Fig. 3(d)] is used, which is a stable structure for As-rich surfaces of GaAs(001). As a standard for the energy, the (2×2) ideal structure [Fig. 3(c)] is also adopted as a model.

Besides the above-mentioned *flat* models, some models with higher coverages ($\theta=1.25, 1.50$) and with complex structures, which are not *flat* models, are investigated in Sec. V.

The Brillouin zones (BZ's) used in this work are illustrated in Fig. 5, where Γ - J_1 - K_{11} - J'_1 - Γ , Γ - J_2 - K_{21} - J'_1 - Γ , Γ -

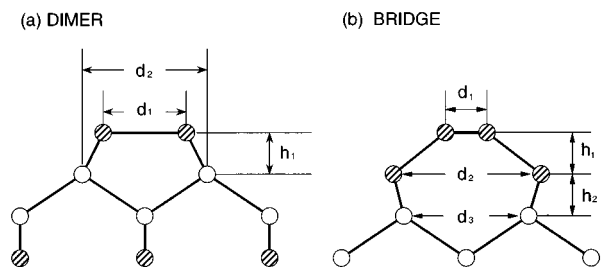


FIG. 4. Schematic illustration of the side views of dimer and bridge models. Hatched and open circles are the atoms on the same plane, respectively.

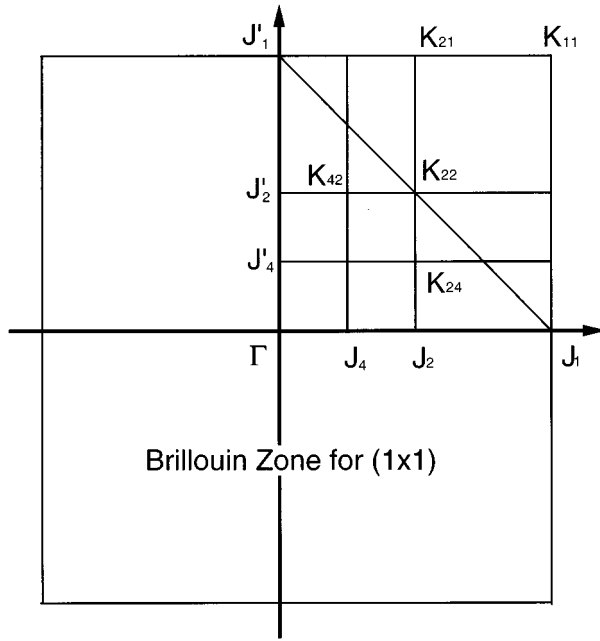


FIG. 5. Illustration of Brillouin zone (BZ) used in this study. Γ - J_1 - K_{11} - J'_1 - Γ , Γ - J_2 - K_{21} - J'_1 - Γ , Γ - J_4 - K_{42} - J'_2 - Γ , and Γ - J_1 - K_{22} - J'_1 - Γ correspond to BZ's of (1×1) , (2×1) , (4×2) , and $c(2 \times 2)$, and so on.

J_4 - K_{42} - J'_2 - Γ and Γ - J_1 - K_{22} - J'_1 - Γ correspond to the BZ's of (1×1) , (2×1) , (4×2) , and $c(2 \times 2)$, and so on.

IV. RESULTS

In this section, the results of the total-energy minimization are presented for B- and N-rich surfaces with various stoichiometries. The stability of surfaces with the same stoichiometry is also compared. Characteristic features of the various surfaces are also discussed. A fundamental problem of compound surfaces would be to determine the phases that are stable under different experimental conditions. For example, in an atmosphere with high N_2 concentration, the c -BN surface will be in a N-rich phase and a B-rich surface will rarely appear. The answer to this problem is assigned to Sec. V A. The calculations are executed in two steps to save computational time as described in Sec. II. In this section, we call the first step a precalculation and the second a *final* calculation.

For GaAs surfaces the validity of the EC rule has been proved in many cases by theoretical and experimental studies.³³ For models of H and S adsorbed on GaAs surfaces, its validity has been also suggested by theoretical studies.⁵⁷⁻⁵⁹ Since c -BN is a III-V semiconductor like GaAs, the EC rule is expected to play an important role in predicting structures for the c -BN(001) surface.

The EC rule (model) is a simple rule (model) to explain reconstructed structures of the tetrahedrally coordinated compound semiconductor surfaces. Fundamental conditions for the EC model are as follows. The total number of electrons is given by a summation of $5/4$ electrons for each tetrahedral bond of a negative atom (N) and $3/4$ electrons for that of a positive atom (B). Two electrons are assigned to each chemical bond and to each dangling bond of a negative

N-rich $\theta=1.0$

(1x1) ideal 0.00 eV (-40.33847 Ht)	(1x1) relaxed -0.20 eV
(2x1) dimer -1.39 eV	(1x2) bridge I -0.24 eV
c(2x2) ideal 0.00 eV (-40.33840 Ht)	c(2x2) dimer -1.14 eV
c(2x2) bridge I -0.13 eV	c(2x2) bridge II To bridge I

FIG. 6. Result of the total-energy minimization of N-rich ($\theta=1.00$) full coverage reconstructed surfaces. The total energies are described in units of $eV/(1 \times 1)$. All models here do not satisfy the EC model and show the metallic or semimetallic feature. See text.

atom (N) and all dangling bonds of positive atoms remain empty. If the number of electrons available matches the number required by the EC rule, the model is an EC model. The EC rule means that an EC model will be semiconducting and stable from the viewpoint of the total energy. In the case of c -BN(001) surfaces, it is important to examine the validity of the EC model with a first-principles study, because the EC model provides an intuitive picture for large systems and adsorption on surfaces without massive calculations.

For convenience, unless otherwise noted, the energies mentioned below are those for a (1×1) unit cell. The results of total-energy minimizations are summarized in Figs. 6, 10, 11, 13, 15, 18, corresponding to the stoichiometries given, where E and S denote that the model satisfies the EC model and is semiconducting, respectively. In these figures the schematic illustrations are added for convenience, where open and closed circles denote the atoms in the first and the second layers, respectively. The values in the parentheses denote the absolute values of the total energy of the reference model, which is the origin of the energies for the surfaces with the same coverage. When the energies of the models with rectangular cells such as (1×1) , (2×1) , etc. are compared to those for the $c(2 \times 2)$ cell, the different configuration of meshes in real and reciprocal spaces might cause error. To estimate such an error, some of the figures show two equivalent models in the different unit cells and the total energies in parentheses, for example, $N(1.00)c(2 \times 2)$ ideal and $N(1.00)(1 \times 1)$ ideal. From these values we can estimate the error as $\sim 1 \times 10^{-4}$ Hartree, which has no effect on our discussion.

A. Dimer and bridge structures

The dimer structures are popular among the (001) surfaces of tetrahedral coordinated semiconductors such as C, Si, Ge, GaAs, etc. Besides the dimer structures, a semiempirical study²⁹ suggested that bridge structures are more stable in (2×1) and (2×2) unit cells than the dimer structures for c -BN(001). The bridge structures were originally suggested

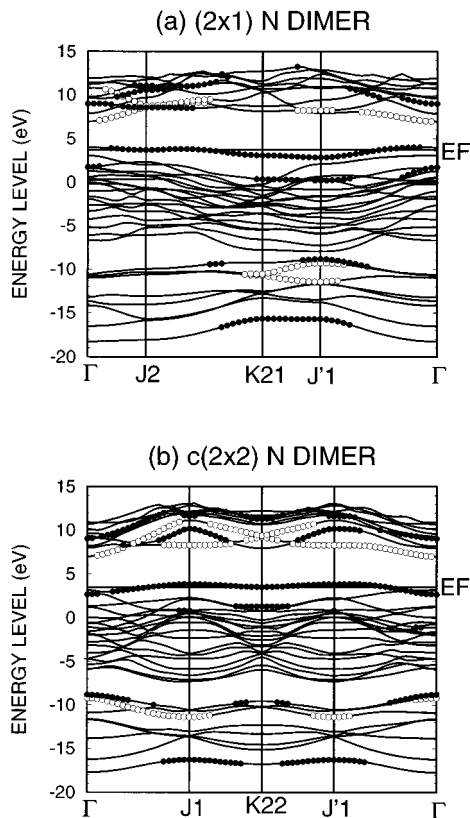


FIG. 7. Band structures of the nitrogen symmetric dimer (a) in (2×1) and (b) in $c(2 \times 2)$, respectively. Closed and open circles denote the orbitals having large amplitudes at the N surfaces and the H terminators.

as a model for the carbon-terminated SiC $c(2 \times 2)$ surface by experiments³⁰ and semiempirical calculations.³¹ Therefore, considering the original structures of SiC, we examine the relative stabilities of the symmetric and the asymmetric

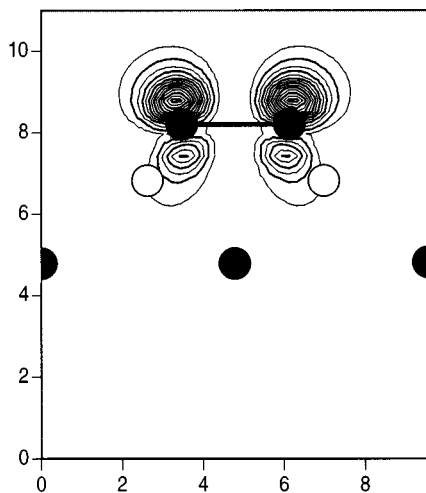


FIG. 8. Contour plot of the squared amplitude of the partially occupied state at the K_{21} point in the Brillouin zone for the (2×1) N-terminated full converge dimer surface. It can be seen that this state consists of the antibonding level of the dangling bonds. The filled and open circles denote nitrogen and boron atoms, respectively. The line and the top nitrogen atoms are on the cutting plane.

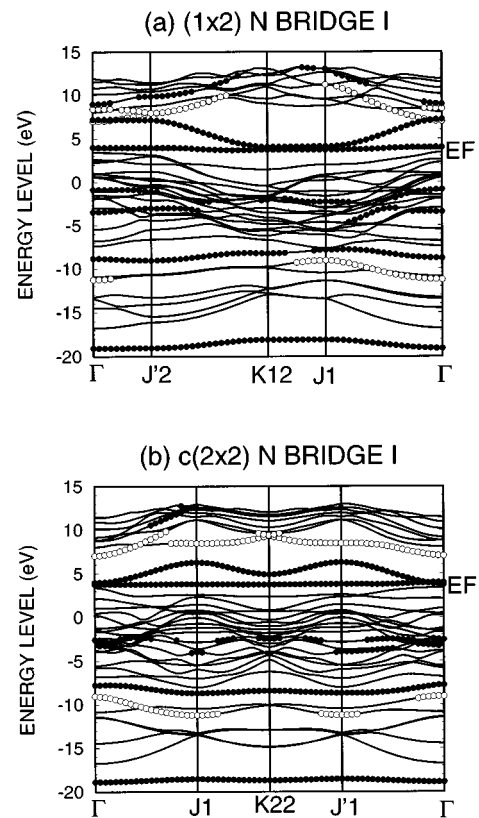


FIG. 9. Band structures of the nitrogen symmetric bridge I (a) in (2×1) and (b) in $c(2 \times 2)$, respectively. Closed and open circles denote the orbitals having large amplitudes at the N surfaces and the H terminators.

structures both of dimer and bridge models of the (2×1) , (1×2) , $c(2 \times 2)$, and (2×2) surfaces. Though starting from several initial asymmetric configurations, both for the dimer and the bridge structures, the models are finally settled to be

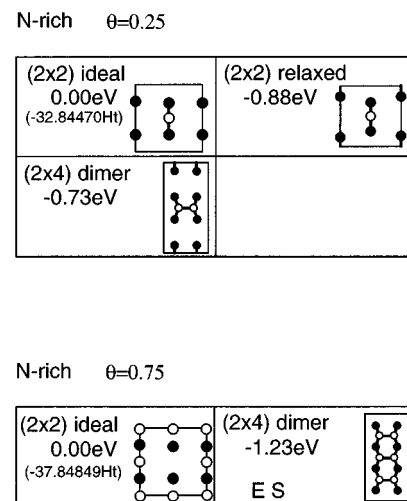


FIG. 10. Result of the total-energy minimization of N-rich ($\theta=0.25$ and 0.75) reconstructed surfaces. The total energies are described in units of $\text{eV}/(1 \times 1)$. In these models E and S represent that the model satisfies the EC model and reveals a semiconducting feature, respectively. See text.

N-rich $\theta=0.5$

c(2x2) ideal 0.00 eV (-35.35798 Ht) E	c(2x2) relaxed -0.82 eV E S
c(2x2) in (2x2) 0.00 eV (-35.35811 Ht) E S	(2x2) dimer -0.58 eV S
(1x2) ideal -0.01 eV E	(1x2) relaxed -0.59 eV E
(2x4) dimer -0.76 eV E S	(4x2) dimer -0.67 eV E S

FIG. 11. Result of the total-energy minimization of N-rich ($\theta=0.50$) half coverage reconstructed surfaces. The total energies are described in units of $\text{eV}/(1 \times 1)$. In these models E and S represent that the model satisfies the EC model and reveals a semiconducting feature, respectively. See text.

the symmetric ones after the total-energy minimization. Furthermore, to make sure, (2×2) bridge and dimer models are investigated, because the asymmetric structures are more favorable in $p(2 \times 2)$ than (2×1) and (1×2) in terms of the bond distortion. However, the asymmetric structures do not exist as far as in the precalculation.

The energy gain of the *asymmetric* buckling dimer, such as in the Si(001) surface, is explained by a mechanism similar to the Haneman model⁶⁰ for the Si(111) surface. A symmetric dimer consists of two equivalent atoms with three σ bonds and one dangling bond. The buckling turns the atoms into different electronic configurations: the atom at the obtuse site has three p^3 -like σ bonds and an s -like dangling bond, and the atom at the flatter site has three sp^2 -like σ bonds and a p -like dangling bond. Since an orbital with an s component has lower energy than that with a p component, an electron is transferred from the dangling bond of the flatter site to that of the obtuse one. This is how the total energy is lowered by the buckling. However, there are two mechanisms for energy loss due to the buckling. One is the energy loss due to the distortion of the bonds between the atoms of the dimer and those in the second layer. The other is losing the energy gain from π - π^* splitting. With respect to the naive bonding picture, the latter is caused by the following mechanism: the charge transfer by the buckling requires breaking of the π bond, resulting in a loss of bonding energy due to π - π^* splitting and an increase in the Hartree energy. Generally, the stability of the asymmetric dimer depends on the balance of the above-mentioned energy gain and loss. From the above discussion, the asymmetric dimer is unstable when the interaction between the atoms of a dimer is large and the back bond is hard to bend. In the case of c -BN(001), the energy levels with bonding and antibonding dangling bonds split for the symmetric dimers as shown in Fig. 7(a) in (2×1) and 7(b) in $c(2 \times 2)$, where closed and open circles denote the orbitals having large amplitudes at the N surfaces and the H terminators, respectively. In Fig. 7, there are four bands below the Fermi level, which have large

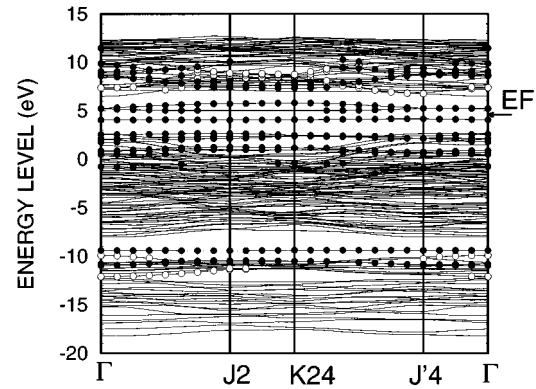


FIG. 12. The band structure of the N-rich (2×4) dimer structure. Closed and open circles denote the orbitals having large amplitudes at the N surfaces and the H terminators. This surface shows semiconducting feature. The Fermi level is indicated by an arrow.

amplitude at the N surface. From the bottom, these bands are characterized as the σ bond between N dimer atoms, back bonds between a dimer atom and an atom in the second layer, and the bonding and the antibonding orbitals of the dangling bonds, respectively. The bonding and antibonding orbitals constitute surface states. The bonding band is found to be well hybridized with the bulk bands. In bulk c -BN, these states are originally in the valence band and emerge into the gap region, because the adjacent boron atoms, which give negative potential to the electron, are removed at a surface. Moreover, as described in Sec. III, the bands derived from the virtual hydrogens are not hybridized with the bands from the other surface atoms. Figure 8 shows a contour map of the upper dangling bond state, the band of which crosses the Fermi energy of the (2×1) dimer structure at the K_{21} points in the Brillouin zone. From the figure, the state is found to be a typical antibonding state derived from the dangling bonds between the nitrogen atoms. Although the above-mentioned bonding mechanism does not hold for the bridge structures, the distortion energy seems large, consid-

B-rich $\theta=1.0$

(1x1) ideal 0.00 eV (-30.33378 Ht)	(1x1) relaxed -0.06 eV
(1x2) dimer -0.97 eV	(2x1) bridge I +0.36 eV
c(2x2) ideal 0.00 eV (-30.33368 Ht)	c(2x2) dimer -0.98 eV
c(2x2) bridge I +0.45 eV	

FIG. 13. Result of the total-energy minimization of B-rich ($\theta=1.00$) full coverage reconstructed surfaces. The total energies are described in units of $\text{eV}/(1 \times 1)$. All models here do not satisfy the EC model and show the metallic or semimetallic feature. See text.

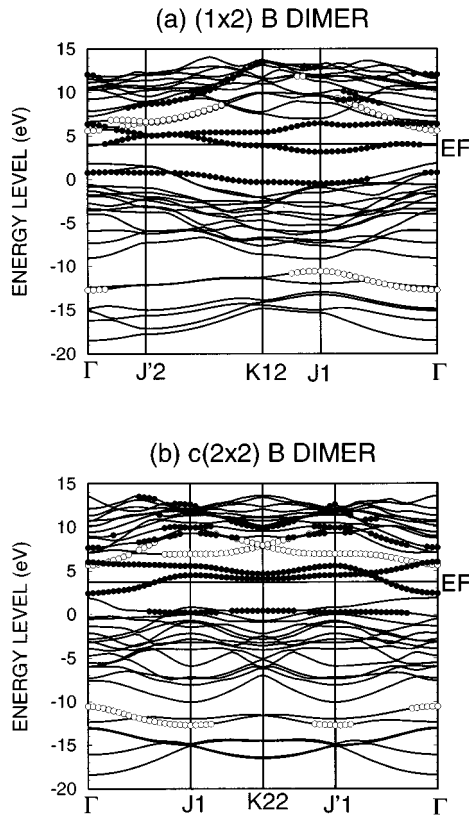


FIG. 14. Band structures of the boron symmetric dimer (a) in (2×1) and (b) in $c(2 \times 2)$, respectively. Closed and open circles denote the orbitals having large amplitudes at the B surfaces and the H terminators.

ering the structure where a nitrogen dimer is inserted into the boron dimer bond in the second layer. The electronic structures of the bridge I in (1×2) and $c(2 \times 2)$ are also presented in Fig. 9. There are several bands having large amplitude in the surface region, which are denoted by closed circles. Among these bands, the two bands at the bottom are bonding and antibonding orbitals derived from s orbitals of nitrogen dimer atoms. At the Fermi level, there is a band with little dispersion, which is half filled.

As described above, in the case of c -BN(001) surfaces, the distortion energy as well as the loss of the π - π^* bonding energy caused by taking an asymmetric structure is large, and this indicates that the symmetric structures are favorable. This is also justified from the total-energy minimization results. Therefore, symmetric configurations are assumed in the following for the dimer and bridge structures. The results of the total-energy minimization for various surface structures are summarized in Fig. 6. Dimer structures are found to be most stable by the total-energy minimization. Among the N dimer structures, the (2×1) configuration is energetically more favorable than the $c(2 \times 2)$ configuration. This is because the $c(2 \times 2)$ symmetry prevents a relaxation of the atoms in the second layer, as shown in Table IV. The table shows that in the (2×1) symmetry the dimer attracts atoms in the second layer and the distance (d_2) between the atoms is reduced from the ideal value 2.53 to 2.28 Å. On the other hand, the corresponding displacement is forbidden in the $c(2 \times 2)$ structure because of the symmetry. This is the reason

TABLE IV. The values determining the dimer and the bridge structures with full coverage from the present calculation. The values d_1 , d_2 , d_3 , h_1 , and h_2 (Å) are defined in Fig. 5. Ideal corresponds to the bulk c -BN.

			d_1	d_2	d_3	h_1	h_2
	Ideal (bulk)		2.53	2.53		0.89	
B	(1×2)	Dimer	1.62	2.56		0.65	
B	$c(2 \times 2)$	Dimer	1.65	2.53		0.72	
N	(2×1)	Dimer	1.39	2.28		0.72	
N	$c(2 \times 2)$	Dimer	1.39	2.53		0.74	
N	(1×2)	Bridge I	1.17	3.29	2.61	1.15	0.84
N	$c(2 \times 2)$	Bridge I	1.18	3.23	2.53	1.23	0.83

for the enhanced stability of the (2×1) cell as compared with that of the $c(2 \times 2)$ cell, though the unit cell of (2×1) is less favorable than that of $c(2 \times 2)$ in terms of the Ewald and Hartree energies, because the negative N dimers in $c(2 \times 2)$ are further separated than those in (2×1) . Thus the N dimers are expected to be arranged regularly in the (2×1) structure. On the other hand, for B dimer structures, since the relaxed configuration of the second layer atoms of (1×2) ($d_2 = 2.56$ Å) happens to be almost the same as that of $c(2 \times 2)$ ($d_2 = 2.53$ Å), the difference of distortion energies is not significant. The $c(2 \times 2)$ dimer is favored due to the electrostatic factor.

All the bridge structures in the (1×2) and (2×2) surfaces are energetically much less stable than the dimer. The energy loss of the bridge structure is probably due to the distortion of the bonds, since the N_2 dimer is inserted into the dimer bond between B atoms in the second layer [see Fig. 4(b)]. This structure, however, may be possible for the C-terminated SiC(001) surface because the covalent radius (R_{cov}) of C (0.77 Å) is much smaller than that of Si (1.17 Å): the ratio $R_{\text{cov}}(\text{C})/R_{\text{cov}}(\text{Si})$ is as small as 0.66 and the C_2 dimer can be inserted between Si atoms without serious distortion of the atoms in the second and deeper layers. On the other hand, the covalent radii of B and N are 0.88 and 0.70 Å,⁶⁰ respectively, and the corresponding ratio, $R_{\text{cov}}(\text{N})/R_{\text{cov}}(\text{B})$, is 0.80. Therefore the bridge structure would be unfavorable. These geometrical differences cause the different structures for the C-terminated SiC(001) and the N-terminated c -BN(001) surfaces. The discrepancy between the results of the semiempirical calculations²⁹ and the present calculation can be attributed to differences between the techniques used.

From the semiempirical calculation, it is suggested that types I and II exist in the bridge structures and that both types I and II are energetically stable to the same extent.²⁹ The bridges I and II are distinguished by the relation between d_2 and d_3 in Fig. 4. In the bridge I model d_2 is larger than d_3 and the opposite relation holds for the bridge II. However, in the present results both are energetically less favorable than the dimer structures and type I is much more stable than type II. Although the type II structure is a local minimum in the precalculation, starting from the type II configuration it settled to type I in the final calculation. Thus type II probably does not exist as a local minimum, or may

B-rich $\theta=0.5$

$c(2 \times 2)$ ideal 0.00 eV (-28.89426 Ht) E	$c(2 \times 2)$ relaxed -1.03 eV E S
$c(2 \times 2)$ in (2×2) 0.00 eV (-28.89440 Ht) E	(2×2) dimer -0.96 eV
(2×1) ideal -0.06 eV E	(2×1) relaxed -0.83 eV E S
(4×2) dimer -0.71 eV S	(2×4) dimer -0.74 eV E S

FIG. 15. Result of the total-energy minimization of B-rich ($\theta=0.50$) half coverage reconstructed surfaces. The total energies are described in units of eV/(1×1). In these models E and S represent that the model satisfies the EC model and reveals a semiconducting feature, respectively. See text.

be a shallow local minimum. From the above results, we adopt the symmetric dimer structure as the fundamental element for constructing models.

B. N-rich surfaces

In this section, we show results for N-rich c -BN(001) surfaces. For N-rich full coverage ($\theta=1.0$), the results are described in Sec. IV A and summarized in Fig. 6.

For N-rich half coverage ($\theta=0.5$), from the results of the precalculation described in Sec. III, both the (2×1) relaxed and the hollow site configurations are energetically unfavorable compared to the ideal $c(2 \times 2)$ structure, where the atoms are located at ideal bulk sites. The ideal $c(2 \times 2)$ structure is adopted as the origin of energy for the half coverage case. The reason for the instability of the hollow sites is that the hollow sites cannot make steady bonds to the surrounding atoms in the second layer. Further the (2×1) symmetry does not allow relaxation of the second-layer atoms. Thus final calculations are not executed for these cases. As shown in Fig. 11, the interesting feature of these surfaces is that the most stable structure is not that containing dimer structures but the relaxed $c(2 \times 2)$ structure. This is explained by the EC model. In the models with half coverage, all models except the (2×2) dimer model satisfy the EC rule. The models with the two lowest total energies satisfy the EC rule and are semiconducting. Although (4×2) and (2×4) cells have many more degrees of freedom to relax than the $c(2 \times 2)$ cells, the total energy of the $c(2 \times 2)$ relaxed model is lowest among the present models. In the case of GaAs(001) surfaces, the model corresponding to the (2×4) dimer model is the most stable one in some region of chemical potential.⁶² This is explained as follows. The EC model requires that all nitrogen dangling bonds should be fully occupied and all boron dangling bonds empty. This electron transfer causes an electrostatic field. Thus the favorable configuration of the positive and the negative dangling bonds is that which recov-

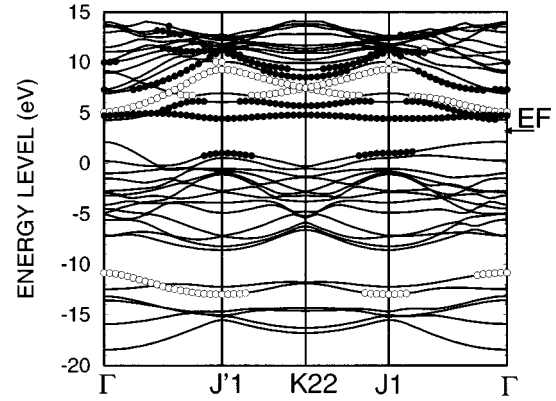


FIG. 16. Band structures of the $c(2 \times 2)$ B-rich reconstructed surfaces with 0.50 coverage. Closed and open circles denote the orbitals having large amplitudes at the N surfaces and the H terminators.

ers electroneutrality in as small a region as possible. For this reason the $c(2 \times 2)$ relaxed model is preferable to the (2×4) dimer model.

For $\theta=0.25$ and 0.75 coverages, among the present models, only the (2×4) dimer structure with $\theta=0.75$ satisfies the EC model and is semiconducting. The results of the total-energy calculations are summarized in Fig. 10. As can be seen in this figure, among the models with $\theta=0.25$, the (2×2) relaxed model has a lower energy than the (2×4) dimer model, though the (2×4) dimer model has more degrees of freedom to relax. This may be because the (2×2) relaxed model contains a small unit satisfying the EC rule, which is the same configuration of the $c(2 \times 2)$ relaxed structure with $\theta=0.5$ in Fig. 11. As will be mentioned in Sec. V, the N-rich models with 0.25 coverage are thermodynamically unstable and will not be realized under equilibrium conditions. However, in some range of chemical potential the (2×4) dimer model with 0.75 coverage, which satisfies the EC model, appears as a stable phase. The band structure of this model is shown in Fig. 12. In this figure, the Fermi level, which is indicated by an arrow, is in the gap and the surface is semiconducting. Two bands just above the Fermi level are derived from the B dangling bond states, which are empty, and below the Fermi level the bands with large amplitude at the surface region, indicated by closed circles, are derived from the nitrogen dangling bonds, which are fully occupied. From the band structure, it is found that the EC rule holds for this model.

C. B-rich surfaces

For B-rich full coverage ($\theta=1.0$), the results of the total-energy minimization are summarized in Fig. 13. For the B-rich surfaces the bridge structures are found to be unstable as was the case for N-rich surfaces. The most stable structure with this stoichiometry contains dimer structures. All of the models with full coverage violate the EC rule. An interesting feature found in the dimer models is that the energy difference between the (1×2) and the $c(2 \times 2)$ dimer models is almost zero. In the N-rich full coverage surfaces the (2×1) model is more stable than the $c(2 \times 2)$ one as described in Sec. IV A. In terms of the Ewald and Hartree terms, the

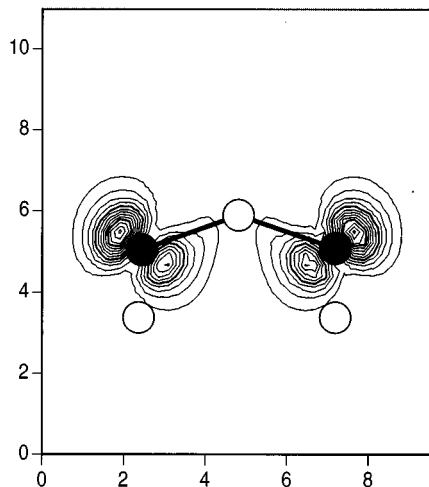


FIG. 17. Contour plot of the squared amplitude of the highest occupied state at the J_1' point in the Brillouin zone for the $c(2 \times 2)$ B-rich reconstructed surface with 0.50 coverage. It can be seen that this state consists of the dangling bonds of the nitrogen atoms in the second layer. The filled and open circles denote nitrogen and boron atoms, respectively. The lines and the top boron atom and the nitrogen atoms in the second layer are on the cutting plane.

dimer structure in the $c(2 \times 2)$ surface has a lower energy than that in the (1×2) surface because the positive B dimer is more uniformly located in $c(2 \times 2)$ than (1×2) . However, the relaxation of atoms in the second layer and the band effects of the surface states show a rather different behavior between N and B surfaces. As can be seen from the distance (d_2) between the atoms in the second layer in Table IV, the relaxed (1×2) structure in the second layer is similar to the relaxed $c(2 \times 2)$ structure and the energy loss in the $c(2 \times 2)$ configuration for B full coverage is much smaller than that for N full coverage. Figure 14 shows the band structure of the (1×2) dimer surface (a) and the $c(2 \times 2)$ dimer surface (b). In this figure, below the Fermi level, the two bands with closed circles correspond to σ and π bonding orbitals between boron dimer atoms, respectively. As seen from the band structure, the dispersion of the π bonding orbitals in the $c(2 \times 2)$ surface is larger than that in the (1×2) surface. This energy gain from the band dispersion contributes to the total-energy lowering of the $c(2 \times 2)$ structure, although a relaxation of the second-layer atoms is forbidden by its symmetry. Therefore, in the B dimer models, the $c(2 \times 2)$ surface tends to be more favorable than the (1×2) surface owing to electronic effects.

For B-rich half coverage surfaces, from the results of the precalculation described in Sec. III, both the (1×2) and the hollow site configurations are energetically unfavorable compared to the ideal $c(2 \times 2)$ structure for the same reason as the N-rich half coverage surfaces in Sec. IV B. Thus the final calculations are not executed for these cases. As shown in Fig. 15, qualitative differences in the electronic features and the total energies among the models used in this stoichiometry are the same as those of the N-rich surface with half coverage. The characteristic feature of these surfaces is that the most stable structure is not that containing dimer structures and satisfying the EC model but the relaxed $c(2 \times 2)$

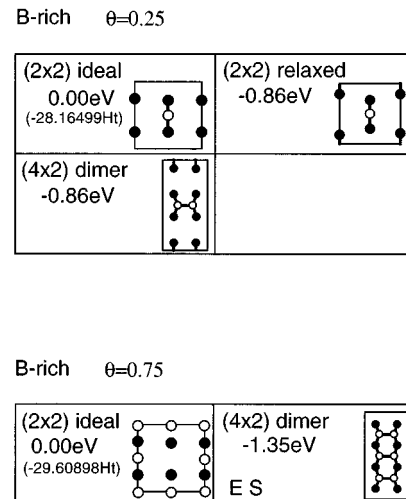


FIG. 18. Result of the total-energy minimization of B-rich ($\theta=0.25$ and 0.75) reconstructed surfaces. The total energies are described in units of $\text{eV}/(1 \times 1)$. In these models E and S represent that the model satisfies the EC model and reveals a semiconducting feature, respectively. See text.

structure. This is explained by the EC model. In these half coverage models, all the models except the (2×2) dimer model satisfy the EC rule. Although the (4×2) cells have many more degrees of freedom to relax than the $c(2 \times 2)$ cells, the total energy of the $c(2 \times 2)$ relaxed model is the lowest among the present models. This is explained as in the case of nitrogen surfaces. The EC model requires that all the nitrogen dangling bonds should be fully occupied and all the boron dangling bonds empty. This electron transfer causes an electrostatic field. Thus the favorable configuration for the positive and negative dangling bonds is that which recovers electroneutrality in a region as small as possible. For this reason, the $c(2 \times 2)$ relaxed model is preferable to the (2×4) dimer model. As will be discussed in Sec. V, the $c(2 \times 2)$ B-rich relaxed structure is realized in a certain region of the nitrogen chemical potential. Its band structure is shown in Fig. 16. Figure 17 shows the top valence state in the J_1' point in the zone. As expected from the EC rule, the

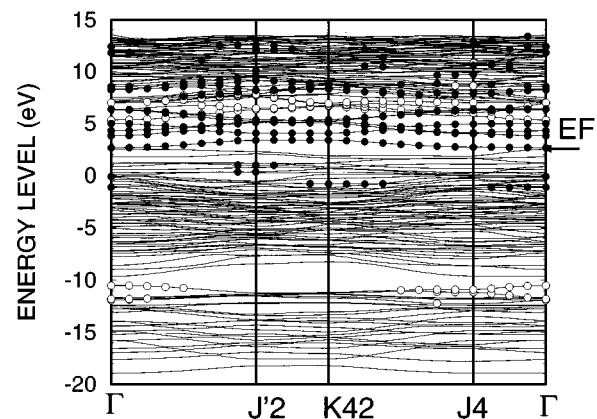


FIG. 19. The band structure of the B-rich (4×2) dimer structure. Closed and open circles denote the orbitals having large amplitudes at the B surfaces and the H terminators. This surface shows semiconducting feature. The Fermi level is indicated by an arrow.

highest level in the valence band consists of the dangling bonds in the electronegative (N) atoms.

For B-rich $\theta=0.25$ and 0.75 coverages, the results of the total-energy calculation are summarized in Fig. 18. Among the present models with the coverage $\theta=0.25$ and 0.75 , only the (4×2) dimer structure with $\theta=0.75$ satisfies the EC rule and is semiconducting, as is the case of N-rich surfaces with $\theta=0.25$ and 0.75 . As can be seen in Fig. 18, among the models with $\theta=0.25$, the (2×2) relaxed model has almost the same energy as the (4×2) dimer model, though the (4×2) dimer model has more degrees of freedom to relax. This may be because the (2×2) relaxed model contains a small unit satisfying the EC model, which is the same configuration as the $c(2\times 2)$ relaxed structure with $\theta=0.5$ in Fig. 15. As will be discussed in the last section, the (4×2) B-rich dimer structure with 0.75 coverage is realized under the condition of a low chemical potential of a nitrogen atom and its band structures are shown in Fig. 19.

V. DISCUSSION

A. Stable structures in c -BN(001)

In this section, the change of stable surface structures is discussed under different chemical potential environments, based on the results of the total-energy minimization of the models with various stoichiometries in Sec. IV. Since c -BN is a compound of two elements, B and N, both B-rich and N-rich surfaces can be realized with various stoichiometries. The chemical potential will determine the relative stability of the models with different stoichiometries. In first-principles studies, methods using the chemical potential were adopted for the GaAs surface phases and gave consistent results with experiments.^{63–65} In the present study, various effects are assumed to be indirectly taken into account through the chemical potential. Assuming the surface is in equilibrium with the bulk, the following relation holds: $\mu_N + \mu_B \approx E_{c\text{-BN}(\text{bulk})}$. The allowed range for μ_N can be determined as follows. As the chemical potential μ_N increases, the nitrogen gas condenses to the bulk phase in the end. Thus

the maximum value of μ_N is determined by the total energy of $\alpha\text{-N}_2$ ($\mu_N \leq \mu_{\text{N}(\text{bulk})}$), which is the ground state of bulk nitrogen as described in Sec. II. The same relation holds for boron ($\mu_B \leq \mu_{\text{B}(\text{bulk})}$). From the above relations, we obtain the following range for the chemical potential of a nitrogen atom: $\mu_{\text{N}(\text{bulk})} - H_f \leq \mu_N \leq \mu_{\text{N}(\text{bulk})}$, where H_f is the heat of formation, calculated to be 3.2 eV, which is defined as $E_{\text{B}(\text{bulk})} + E_{\text{N}(\text{bulk})} - E_{c\text{-BN}(\text{bulk})}$.

As in Refs. 63–65, we approximate the surface free energy by the total energy of the surface E_{surf} . A surface formation energy σ can be defined by a difference between thermodynamic functions for the relevant and standard models as

$$\begin{aligned} \sigma &= E_{\text{surf}}(N_B, N_N) - E_{\text{surf}}^0(N_B^0, N_N^0) - n_B \mu_B - n_N \mu_N \\ &= E_{\text{surf}}(N_B, N_N) - E_{\text{surf}}^0(N_B^0, N_N^0) - \mu_{\text{N}(\text{bulk})}(n_N - n_B) \\ &\quad - n_B E_{c\text{BN}(\text{bulk})} - \delta \mu_N (n_N - n_B), \end{aligned} \quad (1)$$

where N_B^0 and N_N^0 are the numbers of boron and nitrogen atoms contained in the standard model, which is the B-terminated ideal (1×1) surface. The n_B and n_N are the number differences from the standard model defined by $N_B - N_B^0$ and $N_N - N_N^0$, respectively. The $\delta \mu_N$ is a chemical potential of a nitrogen atom measured from the bulk energy ($\mu_{\text{N}(\text{bulk})}$).

For a given chemical potential, the system with the lowest surface formation energy defined above is realized. Figure 20 shows the surface formation energy σ per (1×1) surface for the models with various stoichiometries ($\theta=0.25, 0.50, 0.75, 1.00$) for both B- and N-rich surfaces as a function of the nitrogen chemical potential $\delta \mu_N$. The upper and the lower limits of the range are delimited by vertical lines in the figure. Although for some stoichiometries a few models have almost the same energy, only the model with the lowest energy is represented in this figure. The origin of the formation energies is that corresponding to the B-terminated ideal (1×1) surface. For convenience, we will use the notation ‘‘A(θ)(Sym)conf,’’ where A, θ , Sym, and conf denote

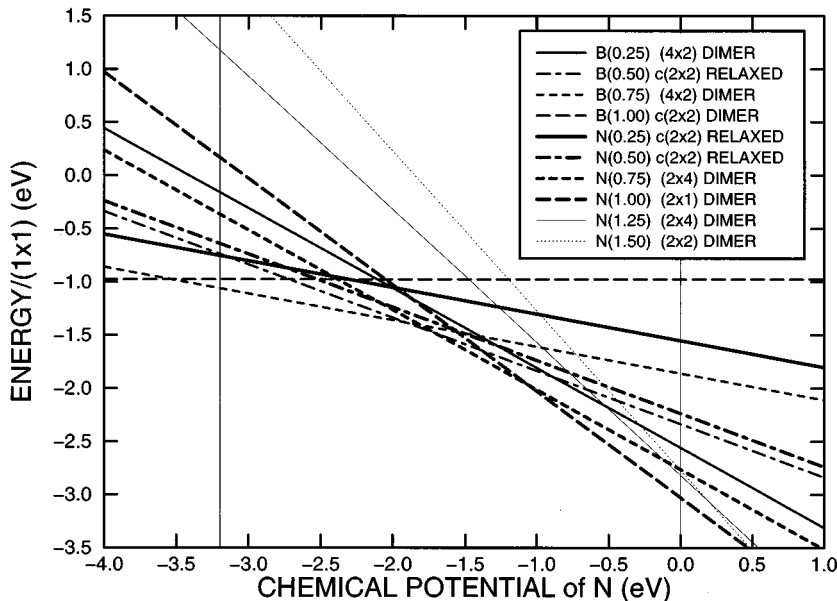


FIG. 20. Formation energies per (1×1) of the c -BN(001) surfaces as a function of a chemical potential of N (μ_N). The origin of μ_N is the energy per an atom of $\alpha\text{-N}_2$, and the allowable range (3.2 eV) is delimited by vertical lines. The formation energy of the B-terminated ideal (1×1) surface is adopted as the origin of the formation energy. Numbers in parentheses of the legend are coverage rates. In a coverage rate, the formation energy of the model with the lowest energy is displayed.

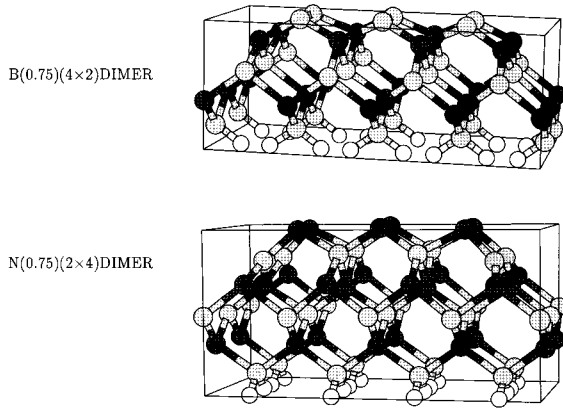
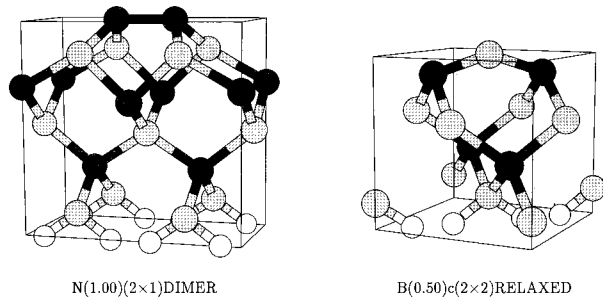


FIG. 21. Perspective views of the model of the stable phases. Dark and light gray circles denote nitrogen and boron atoms, respectively. White circles denote virtual hydrogen atoms. The frames are to guide the eye.

atomic kind (B or N), coverage, unit cell symmetry, and characteristic configuration, respectively. For example, the N-rich full coverage (2×1) dimer and B-rich half coverage $c(2\times 2)$ relaxed structures are represented as N(1.00) (2×1)dimer and B(0.50) $c(2\times 2)$ relaxed, respectively.

From Fig. 20, we can find significant information about the stability of the surfaces. Since the surface is in equilibrium with the bulk, the lines for stoichiometries that can be changed into each other by exchanging a BN pair have the

$$N(1.00)(2\times 1)\text{dimer}(\mu_{N(\text{bulk})} - 1.06 \text{ eV} \leq \mu_N \leq \mu_{N(\text{bulk})}) \quad (\text{I})$$

$$\rightarrow N(0.75)(2\times 4)\text{dimer}(\mu_{N(\text{bulk})} - 1.70 \text{ eV} \leq \mu_N \leq \mu_{N(\text{bulk})} - 1.06 \text{ eV}) \quad (\text{II})$$

$$\rightarrow B(0.50)c(2\times 2)\text{relaxed}(\mu_{N(\text{bulk})} - 1.91 \text{ eV} \leq \mu_N \leq \mu_{N(\text{bulk})} - 1.70 \text{ eV}) \quad (\text{III})$$

$$\rightarrow B(0.75)(4\times 2)\text{dimer}(\mu_{N(\text{bulk})} - 3.20 \text{ eV} \leq \mu_N \leq \mu_{N(\text{bulk})} - 1.91 \text{ eV}) \quad (\text{IV}).$$

The perspective views of the stable phases are shown in Fig. 21. The above phases are ordered from the highest chemical potential to the lowest. Phase (I) is the most stable phase of the highest chemical potential for a nitrogen atom in the present study. In the phase (II) and (IV) regions, the missing dimer structures with 0.75 coverage for N- and B-rich surfaces are stable. The B(0.50) $c(2\times 2)$ relaxed surfaces can be observed in the narrow range in phase (III). This

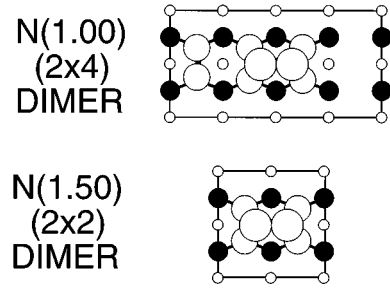


FIG. 22. N(1.00)(2×4)dimer: an EC model for N(1.00), which has lower energy than the (2×1) dimer in the case of GaAs cases. N(1.50) (2×2)dimer: the top view of a N(1.50) model for adsorption and dissociation. See text.

same slope. Thus both the B-rich 0.25 coverage and the N-rich 0.75 coverage surfaces have the same slope and the line corresponding to the N-rich surface is under that of the B-rich surface. Therefore the B-rich 0.25 coverage surfaces are never realized under equilibrium conditions. Similar results can be also derived for the B-rich and the N-rich 0.50 coverage surfaces, and for the B-rich 0.75 and N-rich 0.25 coverage surfaces. For the reason mentioned above, the N-rich 0.50 coverage surfaces and the N-rich 0.25 coverage surfaces are unstable and never realized under equilibrium conditions. These results can be partially understood by the EC model, since the models with 0.25 coverage do not satisfy the EC rule.

A remarkable feature over the range of the above chemical potential μ_N is the extraordinary stability of the N-terminated surfaces with full coverage. Considering the allowed range of the chemical potential, the B-terminated surfaces with full coverage will not be realized. On the other hand, the N-terminated surfaces are stable over a wide range of μ_N as $\mu_{N(\text{bulk})} - 1.1 \text{ eV} \leq \mu_N \leq \mu_{N(\text{bulk})}$. It should be noticed that this structure is metal in spite of its stability. This difference between GaAs and c -BN can be understood by the strong bonding between the nitrogen and boron atoms.

From Fig. 20, we can predict the transition of the surface phases in terms of the chemical potential as

region is subtle and phase (III) competes with phases (II) and (IV). Therefore around this chemical potential range, the surfaces may reveal a complex mixed phase.

As shown in Fig. 21, the models obeying the EC rule, that is N(0.75) (2×4) dimer, B(0.50) $c(2\times 2)$ relaxed, and B(0.75) (4×2) dimer reveal characteristic local structures. The structure including the threefold coordinated boron atom tends to be flat and sp^2 -like, in order to increase the s com-

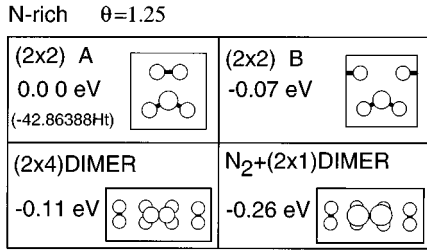


FIG. 23. Result of the total-energy minimization of N-rich ($\theta=1.25$) coverage reconstructed surfaces. The total energies are described in units of eV/(1 \times 1). The origin of total energy is that of the reconstructed (2 \times 2)A model. N₂+(2 \times 1)dimer means N₂ in the vacuum region and (2 \times 1) dimer in (4 \times 2) unit cell.

ponent of the occupied orbitals. In the case of the threefold coordinated nitrogen atoms, these atoms takes p^3 -like structures and the s component of the dangling bond increases.

B. Validity of the electron counting rule in *c*-BN(001)

In order to apply the electron counting (EC) rule to the *c*-BN surfaces, it is necessary to understand its limitations. Therefore in this section we will discuss the validity and the limits of the EC rule.

The EC rule is based on a simple tight-binding picture in which the total energy of the system can be reduced by electron transfer from the electropositive atoms to the electronegative atoms, because the energy levels of dangling bonds for an electronegative element are lower than those for an electropositive element. According to this picture, the system satisfying the EC rule, which is described briefly in Sec. IV, should be semiconducting and energetically stable. It is expected that the EC model holds for *c*-BN more efficiently than GaAs, because the electronegativities of B, N, Ga, and As are 2.0, 3.0, 1.6, and 2.0, respectively,⁶⁰ and the difference between B and N is 1.0, which is larger than that between Ga and As (0.4). From the results for the flat models in Sec. IV, it is found, as expected, that the EC rule plays a very important role in determining the stable structure of *c*-BN surfaces. The stable models, in the range of the N chemical potential (II)–(IV) in Sec. IV, are all semiconducting EC models. In the case of the region (I), EC models are not available for N(1.00) within the *flat* models.

Next to the EC rule, the electrostatic energy is the most important influence for determining the stable reconstructed structures, which is demonstrated most remarkably in the boron half coverage case (Fig. 15). For B(0.50), three models satisfy the EC rule. Although the (2 \times 4) structure has more degrees of freedom for reconstruction, it has higher energy than the *c*(2 \times 2) and (2 \times 1) relaxed structures. This suggests that the structure that reduces the electrostatic energy is favored. The importance of the electrostatic energy can be explained from the large difference of the electronegativity between the boron and nitrogen atoms. In other words, the surface structure recovering electroneutrality in as small an area as possible tends to be favored to reduce the electrostatic energy, because any surface reconstructions of EC models will cause charge transfer. A similar trend is also found in N(0.50).

By means of CVD and PVD, the growth of *c*-BN is performed in an atmosphere containing atomic and molecular

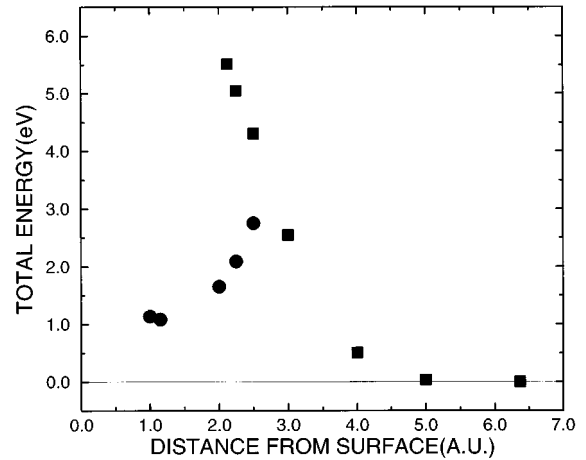


FIG. 24. Energy potentials through adsorption and dissociation paths, which are indicated by squares and circles, respectively, of N₂ on (2 \times 2) N dimer surface. See text.

nitrogen. Therefore we further investigate the N-rich region. For N(1.00), no EC models exist among our flat models. However, getting rid of the *flat* condition, we can construct EC models such as the N(1.00) (2 \times 4) dimer shown in Fig. 22, which have lower energy than the (2 \times 1) dimer model shown in Fig. 6 in the case of GaAs.⁶⁵ Nevertheless, unlike GaAs, this EC model has 0.42 eV/(1 \times 1) higher energy than the (2 \times 1) dimer model. This suggests that the energy difference between N-B and N-N bonds connecting N atoms in the top to the second layer is much larger than the energy gain from the EC model. To make this point clear, we investigate adsorption of N on the N-rich full coverage surface, which includes the N-rich surfaces with more than full coverage.

For N(1.25) coverage, the optimized stable configurations are displayed in Fig. 23. The N(1.25) (2 \times 2) A and B models are those with one N atom inserted between one of the two dimers in N(1.00) *c*(2 \times 2) and N(1.00) (2 \times 1), respectively. Although the *c*(2 \times 2) N(1.00) dimer has higher energy by 0.25 eV than the (2 \times 1) one, the N(1.25) (2 \times 2) B model that is based on the former has lower energy than the A model, mainly because the constraint of *c*(2 \times 2) is released and the B atoms in the second layer are relaxed. Among these N adsorbed models, the (2 \times 4) dimer is the most stable. However, the configuration with N(1.25) coverage will not appear over the allowed range of μ_N as shown in Fig. 20. The total energies of these N adsorbed surfaces are higher by 0.15 eV than the isolated N₂ molecule and a full coverage surface, as shown in Fig. 23, where the total energy of N₂ molecule and N(1.00) (2 \times 1) dimer in (2 \times 4) is shown.

In Fig. 24, we trace the adsorption and the dissociation processes of a N₂ molecule on the (2 \times 1) dimer structure in the (2 \times 2) unit cell, which corresponds to N(1.50) coverage. The top view is shown as N(1.50) (2 \times 2) dimer in Fig. 22. In Fig. 24, the squares and circles indicate the total energies for the adsorption and dissociation processes, respectively. The two different series of the energy surface indicate that the adsorption and the dissociation processes of the simulation correspond to different paths on the energy surface, which do not cross each other. The horizontal axis (z axis) denotes the distance from the surface, whose origin is the top N atom of N(1.00) (2 \times 1) dimer structure. In the adsorption process, the

initial configuration is the N_2 ($z=6.37$ a.u.) and $N(1.00)$ (2×1) dimer in (2×2) and the N_2 approaches the surface from the vacuum region. Holding the tightly bonded structure, the N_2 molecule goes down to the surface and a repulsive force occurs between the N_2 and the surface. As the molecule approaches, the atoms in the surface are pushed down and the energy potential increases. On the other hand, in the dissociation process, the initial configuration is that optimized structure ($z=1.15$ a.u.) and the N_2 goes away from the surface. As the top N_2 leaves from the surfaces, the N atoms of the molecule are each drawn by the surface dimer atoms with two bonds and are separated from each other. This separation causes an increase in the energy potential. At each step, we optimize all the degrees of freedom except the bottom two layers of the slab and the z component of the N_2 , which means that the two N atoms have the same distance from the surface. From these simulations, we found that the adsorption state of N_2 has higher energy by 1.08 eV per molecule than the isolated state, where the N_2 is 6.4 a.u. apart from the top of the dimer, and that the reaction path has a rather large activation barrier, which is roughly estimated as ~ 3 and ~ 2 eV/molecule in the adsorption and the dissociation processes, respectively. These results suggest that the N-N bond between the full coverage N layer and N_2 molecule on the layer is so weak that the system with more than N full coverage decomposes to the full coverage layer and N_2 molecules or N_2 bulk ($\mu_N \rightarrow 0$) in equilibrium.

VI. CONCLUSION

In this work we systematically investigated the c -BN(001) surfaces with various stoichiometries by the local density functional approach with ultrasoft pseudopotentials. The total energy of the models is optimized with respect to the electronic and atomic degrees of freedom by the conjugate gradient method. From the calculated results, we predict that, as the chemical potential decreases from the N_2 bulk value, the stable surface will change as follows: $N(1.00)$ (2×1) dimer, $N(0.75)$ (2×4) dimer, $B(0.50)$ $c(2\times 2)$ relaxed and $B(0.75)$ (4×2) dimer. Due to the difficulty of making wide clean surfaces, diffractive measurements such as LEED give little information on the surface symmetry. However, the above-mentioned phases may be observed by real-space measurements such as STM, AFM (atomic force microscopy), etc., which enable the observation of small clean surface region. Further, we examined the validity of the EC rule, which has been used successfully to determine GaAs surface structures. In the flat models, which contain at most one layer with defects and no interlayer N-N and B-B bonds, the EC rule holds very well, because the stable models are all EC models in the coverage range where we can construct EC models and are semiconducting. From the re-

sults of the flat models, we found that next to the EC rule, the electrostatic energy has the most important role in determining the stable structures. However, from the total-energy calculation of EC models, we suggest that the non-EC model has a lower energy than an EC model made by breaking N-B bonds in N-rich coverage, which is not the case of GaAs(001), because the energy difference between the N-B and N-N bonds is larger than the energy gain obtained by taking the EC model. To confirm this point, we further studied the adsorption and dissociation processes of N_2 on the c -BN(001) surface with full N coverage. It is found that the N_2 adsorption state has higher energy than the isolated N_2 state by 1.08 eV/molecule and that the adsorption and dissociation barrier can be roughly estimated as ~ 3 and ~ 2 eV per molecule, respectively. The EC models mentioned above are not stable energetically. As shown in the stability between $c(2\times 2)$ and (2×1) dimer models in the full coverage B and N surfaces, the degrees of freedom of reconstruction affect the stability in c -BN as well as other semiconducting surfaces such as GaAs, Si, and Ge. Therefore, as the characteristic feature of c -BN(001) surfaces, we suggest that the important factors to determine stable structures are N-B bond saturation, the EC rule, and electrostatic energy, whose effect decreases in this order.

ACKNOWLEDGMENTS

We are indebted to Dr. K. Shiraishi, Professor T. Nakayama, and Professor N. Shima for much useful advice on calculational programs and various discussions. We also thank Dr. T. Ohno for discussions especially on GaAs surfaces. We are grateful to Dr. K. Kobayashi for encouragement and illuminative discussions. One of the authors (J.Y.) thanks Professor A. Kotani for a critical reading of the previous manuscript and fruitful discussions, and also thanks Professor T. Ando, Professor T. Fujiwara, Professor H. Fukuyama, and Professor K. Terakura for stimulating discussions. This work is partially supported by grant-in-aid from the Ministry of Education, Science and Culture of Japan. The numerical calculations were performed by HITAC S-3800 at the Computer Center of the University of Tokyo. We used XMOLE, version 1.3.1, Minnesota Supercomputer Center, Inc., Minneapolis MN, 1993.

APPENDIX

In this appendix, we tabulate the positions of atoms in the reconstructed structures for the stable phases, that is, $N(1.00)$ (2×1) dimer, $N(0.75)$ (2×4) dimer, $B(0.50)$ $c(2\times 2)$ relaxed,

TABLE V. The position of atoms in the N-rich ($\theta=1.00$) (2×1) dimer structure.

	r_1	r_2	r_3		r_1	r_2	r_3		r_1	r_2	r_3
N	0.6371	0.5000	0.3712	N	0.3629	0.5000	0.3712	B	0.7255	0.0000	0.3089
B	0.2745	0.0000	0.3089	N	0.5000	0.0000	0.2173	N	0.0000	0.0000	0.2428
B	0.5000	0.5000	0.1466	B	0.0000	0.5000	0.1595	N	0.7547	0.5000	0.0758
N	0.2453	0.5000	0.0758	B	0.2500	0.0000	0.0000	B	0.7500	0.0000	0.0000

TABLE X. The position of atoms in the B-rich ($\theta=1.00$) (1×2) dimer structure.

	r_1	r_2	r_3		r_1	r_2	r_3		r_1	r_2	r_3
B	0.3399	0.5000	0.2901	B	0.6601	0.5000	0.2901	N	0.2468	0.0000	0.2341
N	0.7532	0.0000	0.2341	B	0.5000	0.0000	0.1506	B	0.0000	0.0000	0.1577
N	0.5000	0.5000	0.0738	N	0.0000	0.5000	0.0787	B	0.2500	0.5000	0.0000
B	0.7500	0.5000	0.0000								

B(0.75) (4×2) dimer, B(1.00) (1×2), and $c(2\times 2)$ dimer structures in Tables V, VI, VII, VIII, IX, and X, respectively.

Although full coverage B-terminated surfaces are not stable in the allowed region of the chemical potential, the positions of the reconstructed surfaces are also tabulated below for comparison. Since the two configuration, $c(2\times 2)$ and (1×2), dimer structures have almost the same total energy in this coverage, positions for both structures are listed.

In the tables, the positions (\mathbf{r}) are represented by fractional coordinates, where the vectors spanning the supercell are taken as unit vectors. The positions in the fractional coordinates (\mathbf{r}) can be transformed into those (\mathbf{x}) in the Cartesian coordinates (atomic units) as $\mathbf{x}=l_0\mathbf{A}\mathbf{r}$, where l_0 and \mathbf{A} are the lattice constant of the bulk c -BN and the matrix that define the supercell in units of l_0 ($=6.76140$). The supercells are spanned the three column vectors of \mathbf{A} . The \mathbf{A} are listed as follows.

For N(1.00) (2×1) dimer (Table V) and B(1.00) (1×2) dimer (Table X),

$$\mathbf{A} = \begin{pmatrix} \sqrt{2} & 0 & 0 \\ 0 & \sqrt{2}/2 & 0 \\ 0 & 0 & 3.25 \end{pmatrix}.$$

For N(0.75) (2×4) dimer (Table VI) and B(0.75) (4×2) dimer (Table VIII),

$$\mathbf{A} = \begin{pmatrix} \sqrt{2} & 0 & 0 \\ 0 & 2\sqrt{2} & 0 \\ 0 & 0 & 3.25 \end{pmatrix}.$$

For B(0.50) $c(2\times 2)$ relaxed (Table VII) and B(1.00) $c(2\times 2)$ dimer (Table IX),

$$\mathbf{A} = \begin{pmatrix} 1 & 0 & 0 \\ 0 & 1 & 0 \\ 0 & 0 & 3.25 \end{pmatrix}.$$

*Present address: Advanced Research Laboratory, Toshiba Corp. 1 Komukai Toshiba-cho, Saiwai-ku, Kawasaki 210, Japan.

†Present address: Advanced Research Laboratory, Hitachi, Ltd. Hatoyama, Saitama, 350-03, Japan.

¹R. H. Wentorf, Jr., *J. Chem. Phys.* **26**, 956 (1957).

²*Synthesis and Properties of Boron Nitride*, edited by J. J. Pouch and S. A. Alterovitz (Trans Tech Publications, Aedermannsdorf, 1990).

³H. Saito, T. Hirose, H. Matsui, Y. Hirotsu, and Y. Ichinose, *Surf. Coat. Technol.* **39/40**, 265 (1989).

⁴S. Shanfield and R. Wolfson, *J. Vac. Sci. Technol. A* **1**, 323 (1983).

⁵M. Satou and F. Fujimoto, *Jpn. J. Appl. Phys.* **22**, L171 (1983).

⁶T. Ikeda, Y. Kawate, and Y. Hirai, *J. Vac. Sci. Technol. A* **8**, 3168 (1990).

⁷V. N. Gashtold, S. A. Kutolin, L. M. Shakarian, L. F. Belova, and G. M. Komarova, *Elektronnaya Tekh. Series* **12** (4), 58 (1970).

⁸C. Weissmantel, K. Bewilogua, D. Dietrich, H.-J. Erler, H.-J. Hinneberg, S. Klose, W. Nowick, and G. Reisse, *Thin Solid Films* **72**, 19 (1980).

⁹K. Inagawa, K. Watanabe, H. Ohson, K. Saitoh, and A. Itoh, *J. Vac. Sci. Technol. A* **5**, 2696 (1987).

¹⁰Y. Andoh, S. Nishiyama, H. Kirimura, T. Mikami, K. Ogata, and F. Fujimoto, *Nucl. Instrum. Methods B* **43/44**, 128 (1990).

¹¹M. Murakawa and S. Watanabe, *Surf. Coat. Technol.* **43/44**, 128 (1990).

¹²S. Koizumi, T. Murakami, and T. Inuzuka, *Appl. Phys. Lett.* **57**, 563 (1990).

¹³G. L. Doll, J. A. Sell, C. A. Taylor II, and R. Clarke, *Phys. Rev. B* **43**, 6816 (1991).

¹⁴A. Zunger and A. J. Freeman, *Phys. Rev. B* **17**, 2030 (1978).

¹⁵R. Dovesi, C. Pisani, and C. Roetti, *Int. J. Quantum Chem.* **17**, 517 (1980).

¹⁶R. Dovesi, C. Pisani, C. Roetti, and P. Dellarole, *Phys. Rev. B* **24**, 4170 (1981).

¹⁷R. M. Wentzcovitch, K. J. Chang, and M. L. Cohen, *Phys. Rev. B* **34**, 1071 (1986).

¹⁸R. M. Wentzcovitch, M. L. Cohen, and P. K. Lam, *Phys. Rev. B* **36**, 6053 (1987).

¹⁹R. M. Wentzcovitch, S. Fahy, M. L. Cohen, and S. G. Louie, *Phys. Rev. B* **38**, 6191 (1988).

²⁰E. Knittle, R. M. Wentzcovitch, R. Jeanloz, and M. L. Cohen, *Nature* **337**, 349 (1989).

²¹P. K. Lam, R. M. Wentzcovitch, and M. L. Cohen, in *Synthesis and Properties of Boron Nitride* (Ref. 2), p. 165.

²²K. T. Park, K. Terakura, and N. Hamada, *J. Phys. C* **20**, 1241 (1987).

²³Y.-N. Xu and W. Y. Ching, *Phys. Rev. B* **91**, 7787 (1991).

²⁴W. E. Pickett, *Phys. Rev. B* **38**, 1316 (1988).

²⁵J. Furthmüller, J. Hafter, and G. Kresse, *Phys. Rev. B* **50**, 15 606 (1994).

²⁶D. Vanderbilt, *Phys. Rev. B* **41**, 7892 (1990).

²⁷J. Yamauchi and M. Tsukada, in the *22nd International Conference on the Physics of Semiconductors* (World Scientific, Singapore, 1995), Vol. 1, p. 509.

²⁸J. Yamauchi, S. Watanabe, O. Sugino, and M. Tsukada, *Surf. Sci.* **341**, L1037 (1995).

²⁹K. Osuch and W. S. Verwoerd, *Surf. Sci.* **285**, 59 (1993).

³⁰J. M. Powers, A. Wander, P. J. Rous, M. A. Van Hove, and G. A. Somorjai, *Phys. Rev. B* **44**, 11 159 (1991).

- ³¹P. Badziag, Phys. Rev. B **44**, 11 143 (1991).
- ³²D. J. Chadi, J. Vac. Sci. Technol. A **5**, 834 (1987).
- ³³M. D. Pashley, Phys. Rev. B **40**, 10 481 (1989), and references therein.
- ³⁴P. Hohenberg and W. Kohn, Phys. Rev. **136**, B864 (1964).
- ³⁵W. Kohn and L. J. Sham, Phys. Rev. **140**, A1133 (1965).
- ³⁶K. Laasonen, A. Pasquarello, R. Car, C. Lee, and D. Vanderbilt, Phys. Rev. B **47**, 10 142 (1993).
- ³⁷D. M. Ceperley and B. J. Alder, Phys. Rev. Lett. **45**, 566 (1980).
- ³⁸J. P. Perdew and A. Zunger, Phys. Rev. B **23**, 5048 (1981).
- ³⁹N. Troullier and J. L. Martins, Solid State Commun. **74**, 613 (1990).
- ⁴⁰For example, W. H. Press, B. P. Flannery, S. A. Teukolsky, and W. T. Vetterling, *Numerical Recipes* (Cambridge University Press, Cambridge, 1986), and references therein.
- ⁴¹I. Štich, R. Car, M. Parrinello, and S. Baroni, Phys. Rev. B **39**, 4997 (1989).
- ⁴²D. M. Bylander, L. Kleinman, and S. Lee, Phys. Rev. B **42**, 1394 (1990).
- ⁴³M. P. Teter, M. C. Payne, and D. C. Allan, Phys. Rev. B **40**, 12 255 (1989).
- ⁴⁴J. Yamauchi and M. Tsukada, Appl. Surf. Sci. **75**, 58 (1994).
- ⁴⁵J. Yamauchi, K. Kobayashi, and M. Tsukada, Surf. Sci. **306**, 42 (1994).
- ⁴⁶J. A. Venables and C. A. English, Acta Crystallogr. B **30**, 929 (1973).
- ⁴⁷K. P. Huber and G. L. Herzberg, *Molecular Spectra and Molecular Structure IV. Constants of Diatomic Molecules* (Van Nostrand Reinhold, New York, 1979).
- ⁴⁸G. S. Painter and F. W. Averill, Phys. Rev. B **26**, 1781 (1982).
- ⁴⁹T. H. Jordan, H. W. Smith, W. E. Streib, and W. N. Lipscomb, J. Chem. Phys. **41**, 756 (19xx).
- ⁵⁰J. P. Perdew and Y. Wang, Phys. Rev. B **33**, 8800 (1986).
- ⁵¹*Crystal and Solid State Physics*, edited by K. H. Hellwege and O. Madelung, Landolt-Börnstein, New Series, Group III, Vol. 7c (Springer, Berlin, 1982).
- ⁵²B. Morosin, A. W. Mullendore, P. Emin, and G. A. Slack, in *Boron-Rich Solids*, edited by D. Emin, T. Aselage, C. L. Beckel, I. A. Howard, and C. Wood, AIP Conf. Proc. No. 140 (American Institute of Physics, New York, 1986), p. 70.
- ⁵³F. D. Murnaghan, Proc. Natl. Acad. Sci. **30**, 244 (1944).
- ⁵⁴F. Birch, J. Geophys. Res. **83**, 1257 (1989), and references therein.
- ⁵⁵E. Wigner, Trans. Faraday Soc. **34**, 678 (1938).
- ⁵⁶K. Shiraiishi, J. Phys. Soc. Jpn. **59**, 3455 (1990).
- ⁵⁷Shang-Fen Ren and Yia-Chung Chang, Phys. Rev. B **41**, 7705 (1989).
- ⁵⁸Y. Miyamoto and S. Nonoyama, Phys. Rev. B **46**, 6915 (1993).
- ⁵⁹S. Nonoyama, Y. Miyamoto, Y. Aoyagi, and T. Sugano, Phys. Rev. B **47**, 7622 (1993).
- ⁶⁰D. Haneman, Phys. Rev. **121**, 1093 (1961).
- ⁶¹L. Pauling, *The Chemical Bond* (Cornell University Press, Ithaca, 1967).
- ⁶²J. E. Northrup and S. Froyen, Phys. Rev. Lett. **71**, 2276 (1993).
- ⁶³E. Kaxiras, Y. Bar-Yam, J. D. Joannopoulos, and K. C. Pandey, Phys. Rev. B **35**, 9625 (1987).
- ⁶⁴E. Kaxiras, Y. Bar-Yam, J. D. Joannopoulos, and K. C. Pandey, Phys. Rev. B **35**, 9636 (1987).
- ⁶⁵Guo-Xin Qian, R. M. Martin, and D. J. Chadi, Phys. Rev. B **38**, 7649 (1988).
- ⁶⁶T. Ohno, Phys. Rev. Lett. **70**, 631 (1993).